Geophysical Research Letters

RESEARCH LETTER
10.1029/2021GL095226

Interaction Between Stratospheric Kelvin Waves and Gravity Waves in the Easterly QBO Phase

Young-Ha Kim[1] and **Ulrich Achatz**[1]

[1]Institut für Atmosphäre und Umwelt, Goethe-Universität Frankfurt am Main, Frankfurt, Germany

Key Points:

- Kelvin waves affect the longitudinal and vertical distribution of parameterized gravity-wave drag in the stratosphere significantly
- This effect can make contribution to the zonal mean of gravity-wave drag, thereby affecting the quasi-biennial oscillation progression
- Gravity-wave drag modulated by Kelvin waves also alters the Kelvin-wave momentum flux in the middle stratosphere

Supporting Information:

Supporting Information may be found in the online version of this article.

Correspondence to:

Y.-H. Kim,
kim@iau.uni-frankfurt.de

Citation:

Kim, Y.-H., & Achatz, U. (2021). Interaction between stratospheric Kelvin waves and gravity waves in the easterly QBO phase. *Geophysical Research Letters*, *48*, e2021GL095226. https://doi.org/10.1029/2021GL095226

Received 12 JUL 2021
Accepted 24 AUG 2021

Abstract A general circulation model is used to study the interaction between parameterized gravity waves (GWs) and large-scale Kelvin waves in the tropical stratosphere. The simulation shows that Kelvin waves with substantial amplitudes (~10 m s^{-1}) can significantly affect the distribution of GW drag by modulating the local shear. Furthermore, this effect is localized to regions above strong convective organizations that generate large-amplitude GWs, so that at a given altitude it occurs selectively in a certain phase of Kelvin waves. Accordingly, this effect also contributes to the zonal-mean GW drag, which is large in the middle stratosphere during the phase transition of the quasi-biennial oscillation (QBO). Furthermore, we detect an enhancement of Kelvin-wave momentum flux due to GW drag modulated by Kelvin waves. The result implies an importance of GW dynamics coupled to Kelvin waves in the QBO progression.

Plain Language Summary The variability of the tropical atmosphere at altitudes of about 18–40 km is dominated by a large-amplitude long-term oscillation of wind, the quasi-biennial oscillation, which has a broad impact on the climate and seasonal forecasting. This oscillation is known to be driven by various types of atmospheric waves with multiple spatial scales. Using a numerical model, this study reports a process of interaction between those waves on different scales, which has not been illuminated before. The result implies a potential importance of this process in the progression of the quasi-biennial oscillation. Proper model representations of these multiscale waves and tropical convection are required to simulate this process.

1. Introduction

In the tropics, various types of atmospheric waves are generated from convection, which have a broad spectrum from mesoscales to planetary scales (Bergman & Salby, 1994; Lane & Moncrieff, 2008; Ortland et al., 2011). Not only do they contribute to the atmospheric variability on their own spatio-temporal scales but they also play a crucial role in the mean circulation via wave–mean-flow interactions (e.g., Booker & Bretherton, 1967). The latter is manifested by the quasi-biennial oscillation (QBO) in the tropical stratosphere (Baldwin et al., 2001). The QBO represents a large variation in the mean zonal wind, of up to ~50 m s^{-1} depending on the altitude, which is driven by the momentum carried from the lower atmosphere by large-scale equatorial waves and mesoscale gravity waves (GWs) (Dunkerton, 1997; Holt et al., 2016).

Theoretical studies of QBO dynamics have considered interactions of the zonally symmetric flow with tropical wave modes. For instance, in one-dimensional models (in the vertical) of the tropical stratospheric mean flow (e.g., Holton & Lindzen, 1972; Lindzen & Holton, 1968; Plumb, 1977), which have contributed essentially to the current understanding of the QBO dynamics, the forcing of the flow due to each wave mode is formulated as a function of mean wind and characteristics of the wave, being independent of other wave modes. In the real atmosphere, however, different modes such as equatorial waves and mesoscale GWs can encounter each other in the stratosphere, because the convective sources of these waves are ubiquitous in the tropics and equatorial waves have planetary scales. Among the equatorial wave modes, Kelvin waves especially are observed to have large amplitudes (~10 m s^{-1} in the zonal wind; Wallace & Kousky, 1968), which suggests potential for these waves to affect the propagation and dissipation of GWs they encounter. Therefore it will be of great interest to observe such a wave–wave interaction across different scales in the tropics and to examine its impact on the QBO dynamics. However, to the authors' knowledge, this interaction has not been studied in the literature.

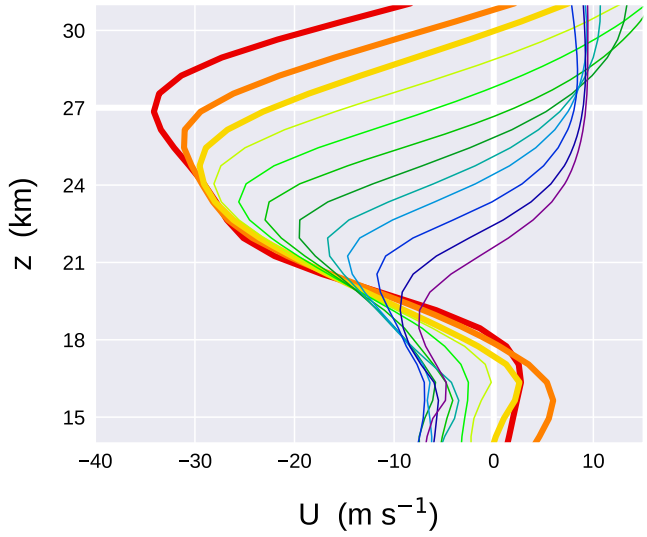

Figure 1. Twelve vertical profiles of zonal-mean zonal wind in the 4-month simulation, averaged for contiguous 10-day intervals from t = 0–10 days to t = 110–120 days (from red to purple in the rainbow color scale). The first three profiles ($t \leq 30$ days) are indicated by thicker lines than the others.

General circulation models (GCMs) may be a useful tool to study the interaction between equatorial waves and GWs, because GW forcing of the large-scale flow is usually parameterized in GCMs and thus easily identifiable. Also, stratospheric Kelvin waves are resolved with reasonable amplitudes and characteristics in current-day GCMs (e.g., Holt et al., 2020; Lott et al., 2009). In this paper, we present a case of interaction between Kelvin waves and GWs, as simulated in a GCM with a state-of-the-art GW parameterization, and discuss its implications for the evolution of the QBO.

2. Methods

The model setup follows Kim et al. (2021). The Icosahedral Non-Hydrostatic (ICON) model (Zängl et al., 2015) is used with its upper-atmosphere extension (Borchert et al., 2019). The horizontal grid spacing is ~160 km, and the vertical spacing is 700 m in the stratosphere. Instead of the operational GW parameterization of this model, we use a prognostic parameterization, the Multi-Scale Gravity Wave Model (MS-GWaM), which predicts the time evolution of GW action density field in position–wavenumber phase space (Achatz et al., 2017; Bölöni et al., 2021; Muraschko et al., 2015). A detailed description of MS-GWaM and its application to ICON is provided in Bölöni et al. (2021). In the current setup, the single-column approximation is used in MS-GWaM, that is, lateral GW propagation is not taken into account. To represent the spectral characteristics and variability of tropical GWs, a subgrid convective source is used in MS-GWaM (Kim et al., 2021).

The model is initialized with the state of May 1, 2010 and integrated for 4 months of which the first 3 months are in the E–W transition phase of the QBO at 20 hPa ($z \sim 27$ km). The zonal-mean zonal winds during the 4 months are presented in Figure 1. We focus on the first month during which the simulated mean flow remains closest to the real atmosphere throughout the stratosphere. In the later 3 months, the evolution of mean flow around 20 hPa seems to be quite similar to that in the observation (not shown), while at lower altitudes the easterly jet becomes weaker than that in the real atmosphere, which is a common bias of existing QBO-simulating models (Bushell et al., 2020; Stockdale et al., 2020).

All the data used and presented in this study are 24-h moving averages of 3-h mean model outputs. The grid-cell outputs are binned zonally with intervals of 2.25° and averaged meridionally within the tropics in each longitude bin by

$$[\psi] = \int_{-\phi_b}^{\phi_b} \psi W \, d\phi \, / \int_{-\phi_b}^{\phi_b} W \, d\phi$$

Here we use a tapering function $W = \exp[-(\phi/\phi_0)^2]$ and set $\phi_b = \phi_0 = 12°$, considering the typical meridional scale of equatorial waves (e.g., Yang et al., 2012). This temporal and meridional averaging filters out the antisymmetric modes of equatorial waves and diminishes signals of resolved waves on relatively small spatio-temporal scales. The equatorial Kelvin waves and the symmetric mode of Rossby waves are sustained which however can be distinguished from each other by the difference in their phase velocities relative to a given mean wind. In our case, Rossby waves are not detected in the lower stratosphere as their propagation is prohibited by the strong easterly wind shear (Figure 1).

3. Results

Figures 2a–2c present Hovmöller diagrams of temperature perturbations (departures from the zonal mean; T') and parameterized zonal GW drag in the tropical lower stratosphere, based on the simulation time (t). Three altitudes, 19, 22, and 28 km, are selected so that the vertical fluctuation of T' is revealed by altered signs between the altitudes. The diagrams exhibit eastward propagation of T' at all these altitudes, most

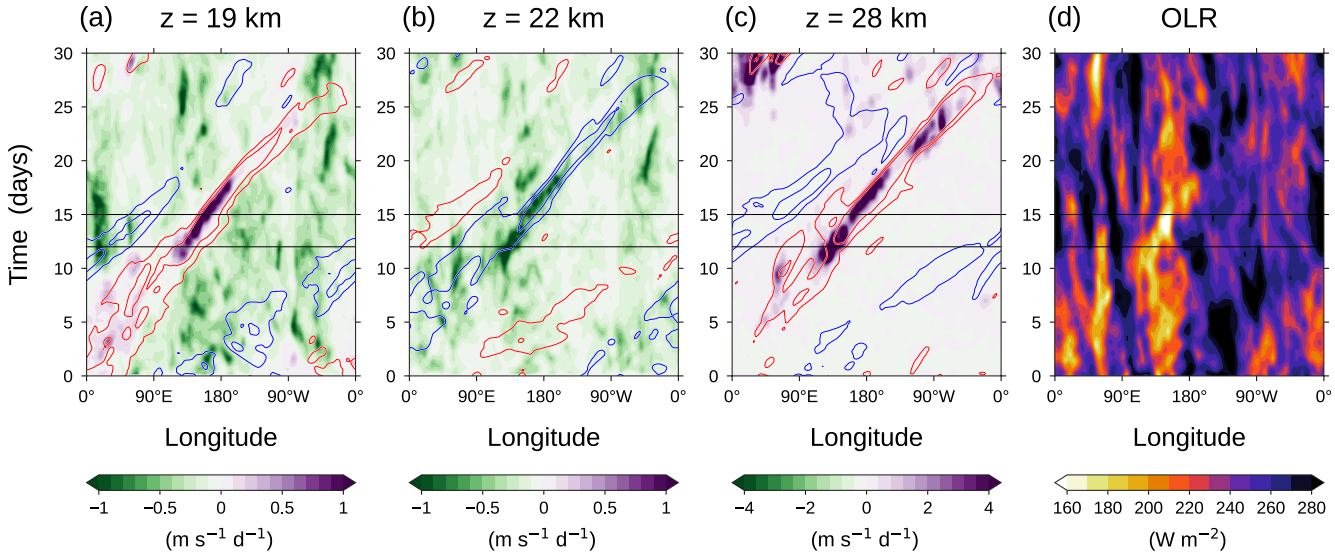

Figure 2. Hovmöller diagrams of (a–c) temperature perturbations (T'; ±2 K and ±4 K, with red and blue contours for positives and negatives, respectively) and zonal gravity-wave drag (shading) at the altitudes of 19, 22, and 28 km (from left to right) and (d) out-going longwave radiation (OLR) for $t \leq 30$ days. The horizontal lines indicate $t = 12$ and 15 days when Figure 3 is plotted.

clearly after $t \sim 10$ days with a phase speed of about 15 m s^{-1}. This phase speed, together with the planetary scale of the perturbations, identifies them as Kelvin waves, according to the equatorial wave theory (e.g., Andrews et al., 1987).

At most locations and time at 19 and 22 km, GWs tend to exert westward force (Figures 2a and 2b) since the QBO is in the easterly shear phase throughout the month at these altitudes (Figure 1). However, eastward GW drag appears at 19 km with substantial magnitudes during $t = 11$–18 days (peaks: 0.9–1.5 m s^{-1} d^{-1}), along the positive T'. Also, at the same locations/time but at 22 km, GW drag is westward and anomalously larger in magnitude than that elsewhere. At 28 km, again the eastward GW drag appears along the positive T' with peaks of 4–8 m s^{-1} d^{-1}, while elsewhere the drag is only weak (the latter is because westward propagating GWs are largely filtered below by strong easterlies of up to –35 m s^{-1} [see Figure 1] and eastward propagating GWs do not induce large forcing in the strong easterly flow at 28 km during the early phase of the E–W transition of QBO). The coupled signals indicate an interaction between Kelvin waves and GWs. The occurrence of positive GW drag at 19 km for the long duration is a strong evidence of the influence of Kelvin waves on GWs, given that it is unlikely to happen in the easterly shear QBO phase unless the flow is perturbed substantially.

On the other hand, to the west of those temperature perturbations, there also exist other prominent perturbations with opposite phases, propagating eastward (around 60°E at $t = 15$ days, Figures 2a–2c). Along those, however, the GW drag is very weak at all altitudes. This is because the convective source of GWs in the troposphere is much weaker at these locations/time, as can be inferred from the out-going longwave radiation presented in Figure 2d as a proxy for deep convection. The asymmetry in the coupling of zonal GW drag and Kelvin wave with respect to the phase implies that the anomalous GW drag coupled with a phase is not averaged out in its zonal mean, and thereby such coupling could potentially play a role in the mean-wind evolution (i.e., QBO). For example, at 28 km (22 km), the GW drag in the narrow longitude band of $[\lambda_0 - 20°, \lambda_0 + 20°]$ contributes by 92% (31%) to the zonal-mean GW drag of 0.28 m s^{-1} d^{-1} (−0.23 m s^{-1} d^{-1}) during $t = 11$–18 days, where λ_0 moves eastward with the speed of 15 m s^{-1} from 120°E at $t = 11$ days. Note that at 28 km, this magnitude of drag is sufficiently large for a significant impact on the mean-wind evolution, given that the total wave forcing driving this early phase of the 20-hPa E–W transition is estimated to be about 0.33–0.5 m s^{-1} d^{-1} in reanalyses (e.g., Kim & Chun, 2015, Figure 12b; Pahlavan et al., 2020, Figure 9b).

The coupling between GW drag anomaly and Kelvin wave shown in Figure 2 is not explained by T' itself but by the local wind shear. The vertical structures of zonal-wind perturbations (u') are presented in Figure 3 along with T' and zonal GW drag at $t = 12$ and 15 days. In addition, the location of maximum vertical

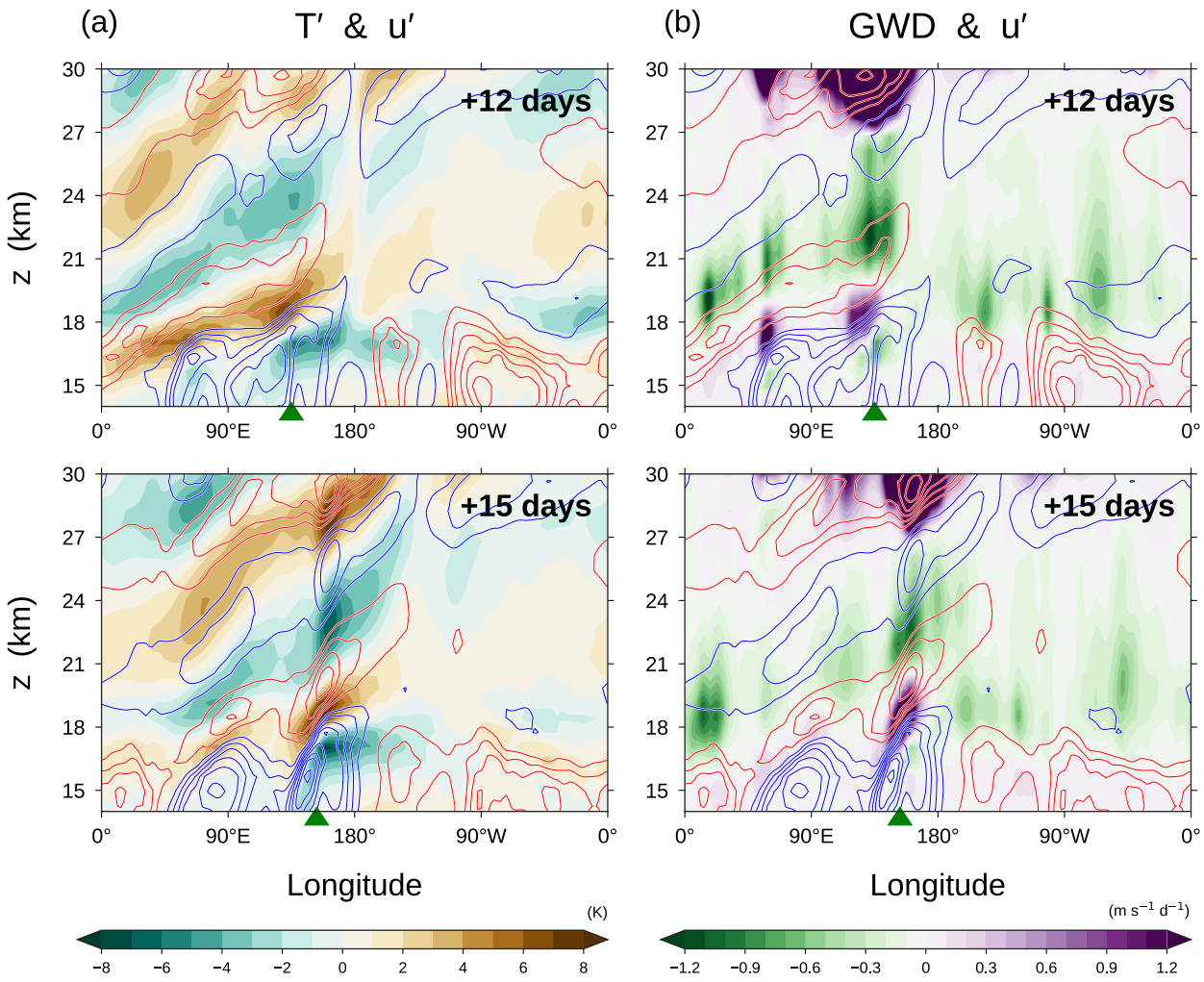

Figure 3. (a) Zonal-wind perturbations (u'; red and blue contours for positives and negatives, respectively, with intervals of 3 m s^{-1}, omitting zeros) superimposed on T' (shading) at t = 12 and 15 days (upper and lower, respectively). At each time, the longitude of maximum upward velocity at z = 14 km is indicated by the green triangle. (b) The same as in (a) but showing the zonal gravity-wave drag instead of T'.

velocity at z = 14 km is indicated. The perturbations in the tropical tropopause layer (z = 14–18.5 km) in Figure 3a show the typical structure of convectively coupled Kelvin waves: at t = 12 days, the negative T' appears above the deep convection (green triangle), while around the top of convection, the flow diverges with large negative u' in the west (e.g., Ryu et al., 2008; Wheeler et al., 2000). In addition, the flow tends to be downward in the region of negative u' away from the convection (not shown). All these perturbations satisfy the Kelvin-wave polarization relation well at $z \sim 17$ km, allowing for vertical propagation of the wave into the stratosphere with considerable amplitudes. The zonal wavenumbers of the simulated Kelvin waves in the stratosphere are mainly 1–2, with a minor secondary peak at ~5 in their spectrum, throughout the period of t = 11–18 days (not shown). The vertical wavelengths are quite long (~10 km) due to the easterly shear throughout the lower stratosphere (Figure 1).

As can be derived from the polarization relation of Kelvin waves, T' is in phase with the vertical shear of u' (u'_z) in the stratosphere (e.g., Andrews et al., 1987, Section 4.7.1). At t = 12 days, the GW drag is exhibited coherently with large magnitudes of u'_z in the lower stratosphere of the eastern hemisphere, but distributed mainly over the regions of strong convection (Figures 3b and 2d). Afterward, the Kelvin waves in the stratosphere exhibit a vertically aligned structure of perturbations, as can be seen in Figure 3a (lower panel) for t = 15 days. These aligned perturbations propagate together until $t \sim$ 24 days (Figures 2a–2c). The relationship between the GW drag and u'_z shown above is maintained for about a week (e.g., for t = 15 days,

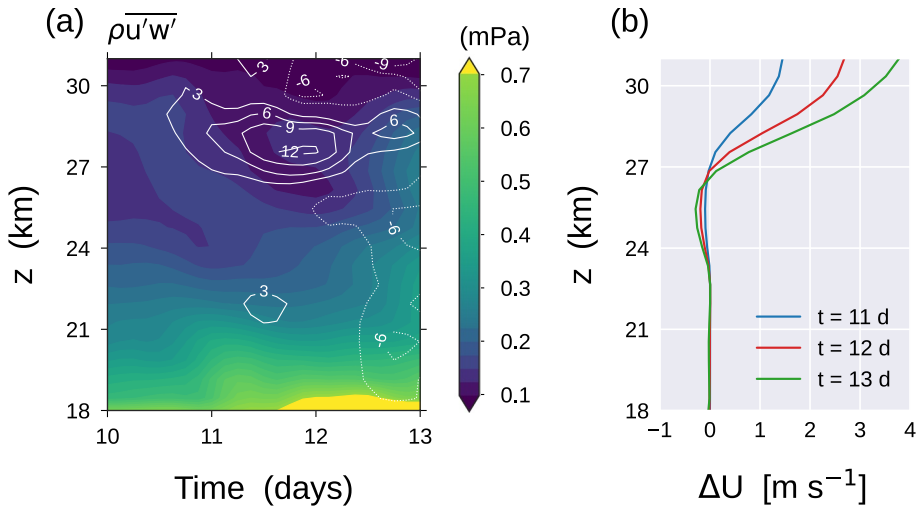

Figure 4. (a) Zonal-mean evolution of perturbation-induced vertical flux of zonal momentum in the original simulation (CTL; shading) and its relative difference between two simulations (CTL – EXPz25; white contours in percentages) for t = 10–13 days. (b) Zonal-mean zonal wind difference (CTL – EXPz25) at t = 11, 12, and 13 days (blue, red, and green, respectively).

see Figure 3b) until the stratospheric Kelvin waves arrive over the eastern Pacific (t ~ 19 days) where the convective source of GWs is weak (Figure 2d).

Figure 3 demonstrates that Kelvin waves of ~10 m s^{-1} amplitudes can perturb the local shear enough to affect the GW drag. This impact may depend on the phases of Kelvin waves where the convection is active in the troposphere. In the current case, the phases of u'_z are positive and negative at z ~ 28 and 22 km, respectively, over the most active convection region (indicated by green triangles in Figure 3), so that they both enhance the local shear of total zonal wind (see Figure 1). The enhanced shear leads to the anomalous GW drag at those altitudes, whereas the GW drag would occur at some higher altitudes if the local shear were not altered by Kelvin waves.

It is interesting to observe that Kelvin waves, which are an important driver of the QBO during the westerly shear phase, can also modulate the GW process that induces westward drag in the opposite phase (at z ~ 22 km in our case). The magnitude of the GW drag coupled to the Kelvin wave in the lower stratosphere is relatively small in the simulation (locally ~1 m s^{-1} d^{-1} at z ~ 22 km, Figure 3), compared to that at higher altitudes. However the aforementioned bias of weak easterly jet in later months (Section 2) suggests that the westward GW drag parameterized in the lower stratosphere might be generally underestimated. The coupling of GWs and Kelvin waves in the easterly shear layer merits future study using a model that resolves and/or parameterizes lower stratospheric GWs with realistic amplitudes.

According to the Kelvin-wave polarization relation, the local tendency of u' is in phase with u'_z which tends to have the same signs with GW drag anomalies (Figure 3). It implies that the Kelvin-wave amplitude can be reinforced by GW drag. We observe a moderately high correlation between the GW drag anomaly and 5-day tendency of u' (Pearson correlation coefficients of 0.4–0.6 at most altitudes above 17 km), which supports the potential for the GW impact upon Kelvin waves. In order to investigate this impact, additional simulations are performed, each of which has the same setup as the original simulation except that, from t = 10 days on, GW forcing to the model dynamics is artificially suppressed to zero in the altitude range [z_0,35 km] in the tropics, where z_0 varies among the simulations from 19 to 25 km (see Supporting Information S1 for details of the setup).

Figure 4a presents the zonal average of perturbation-induced momentum flux in the simulation with z_0 = 25 km (EXPz25) and its difference from the original simulation (CTL). Not surprisingly, the results at t = 10–12 days are nearly identical between the simulations below 25 km (z_0). However, the flux at ~28 km is found to differentiate between the two simulations gradually for the 2 days, showing up to 12% larger flux in CTL than in EXPz25. It demonstrates that the GW drag above 25 km amplifies Kelvin waves at ~28 km

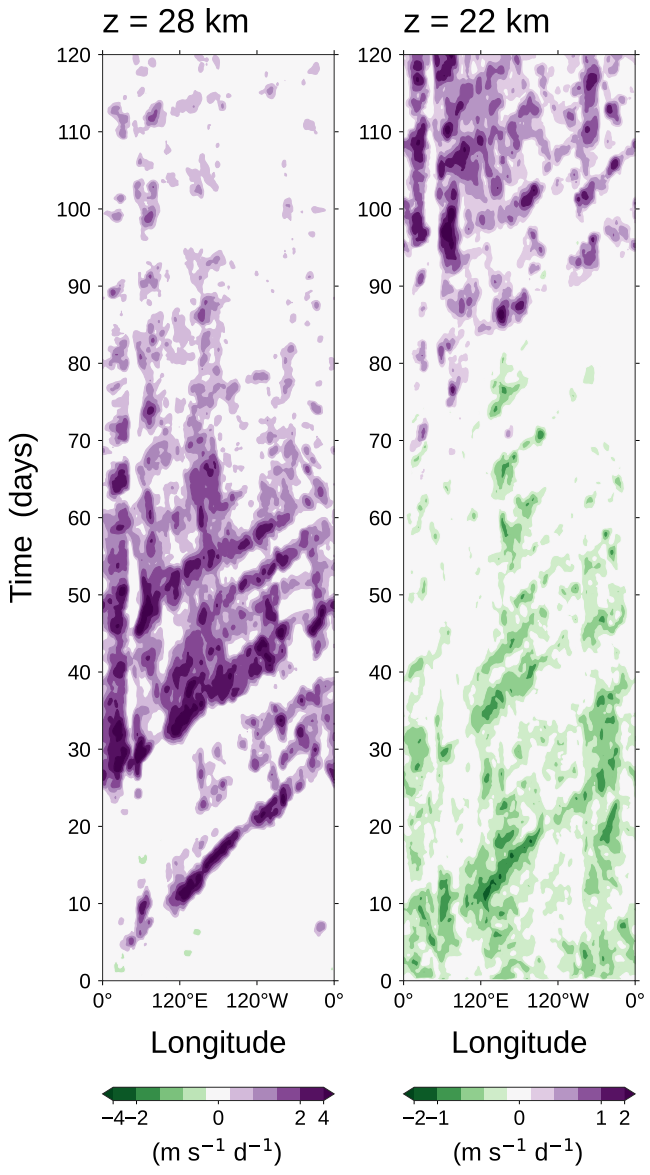

Figure 5. Hovmöller diagrams of zonal gravity-wave drag for t = 0–120 days at the altitudes of 28 and 22 km (left and right, respectively). The base-2 logarithmic scale is used for the shading intervals.

in CTL. Meanwhile, the zonal-mean wind there is also altered by the GW drag, as can be seen by its difference between the simulations shown in Figure 4b. The easterly mean wind at 28–30 km (Figure 1) is weakened by the eastward GW drag in CTL, which results in a reduction of vertical wavelengths of Kelvin waves, thereby enhancing the radiative dissipation of waves. This may be the reason that the increase of momentum flux in CTL is confined to $z < 30$ km where the mean-wind change is only moderate (Figure 4).

After t = 12 days, the mean wind at 28–30 km changes further (Figure 4b), and also the tropospheric flow fields associated with convection begin to differentiate (unpredictably) with noticeable magnitudes between the simulations (not shown). These seem to cause the differences in the momentum flux throughout the stratosphere at $t \sim 13$ days seen in Figure 4a, while preventing further amplification of Kelvin waves around 28 km in CTL. Results in other simulations with z_0 = 22 or 19 km were similar to those in EXPz25 even at $z < 25$ km (not shown), implying that the impact of lowermost stratospheric GW drag on Kelvin waves is negligible in the short term, due probably to the small magnitudes of drag.

In the later 3 months, stratospheric Kelvin waves in the simulation tend to have smaller amplitudes than those in the first month (not shown). There are a couple of reasons for this. In the troposphere, convectively coupled Kelvin waves in the simulation were less active in these months than before, which might partly affect the activity of stratospheric waves (Maury et al., 2013). Also, in the lower stratosphere, the easterlies become weaker with the QBO progression as shown in Figure 1 (even more than in the real atmosphere), which result in a reduction of vertical wavelengths of Kelvin waves. The vertical grid spacing of the current simulation (700 m) might still be not small enough to fully resolve relatively short waves, given the numerical dissipation of the model.

Figure 5 shows the Hovmöller diagrams of zonal GW drag for t = 0–120 days at 28, 25, and 22 km. Despite the smaller amplitudes of simulated Kelvin waves at $t > 30$ days discussed above, signatures of coupling between Kelvin waves and GW drag are found rather persistently during the course of the E–W transition (Figure 1), as can be seen by the drag exhibiting eastward progressions with planetary scales (although they are less clear at 22 km when quasi-stationary or westward signals also seem to exist together). This feature may imply a potential importance of the coupled dynamics of Kelvin waves and GWs during this transition phase of QBO. There also exists the negative GW drag coupled to Kelvin waves at 22 km beyond the first month, although its magnitude is very small.

4. Discussion

The current study shows that stratospheric Kelvin waves with amplitudes of ~10 m s^{-1} strongly affect the distribution of GW drag by modulating the local shear. Furthermore, zonal asymmetry in the distribution of the GW source (convection) can cause this effect to also appear in the zonal mean of the GW drag, thereby influencing the progression of the QBO. The zonal-mean effect may be large especially when a Kelvin wave propagates over an organized convective system that also moves eastward, so that GWs generated from the convection can induce the drag within a certain phase of the Kelvin wave constantly for several days. This may not be a rare case, as organized convective systems often move at the typical phase speed of Kelvin waves and the typical zonal wavelengths of Kelvin waves are large enough to cover a convective

organization in a phase. Such an example is presented in our case during t = 11–18 days (Figures 2 and 3). It is noteworthy that Kelvin waves can also contribute to the easterly momentum deposition of GWs in the lower stratosphere with easterly shear, although the magnitude of GW drag was only small at that altitude (~22 km) in our simulation (Figure 5).

On the other hand, GWs in the middle stratosphere (~20 hPa) are found to influence Kelvin waves when they are coupled. In our case, Kelvin waves are amplified by ~10% (in terms of the zonal-mean momentum flux) in 2 days due to the coupled GW drag (Figure 4). It is difficult to project such an effect to longer time scales, as the GWs also alter the mean wind by which Kelvin waves are largely affected. The impact of GWs on Kelvin waves (and other equatorial waves) may merit further investigation, beyond this case study, by theoretical work or idealized modeling. It also remains to study the coupling of waves in the real atmosphere.

The result revealed complex interactions among GWs, Kelvin waves, and zonal-mean flow as well as convection. It stresses the importance of proper representation of all these in realistic QBO simulation. As the flow modulated by Kelvin waves can be regarded as the mean flow for GWs, the interaction processes are viewed in the context of a GW-mean-flow problem which, in GCMs, should be taken into account by GW parameterization. In the parameterization, description of the flow-dependent source of GWs associated with convection matters. Note that had the GW source been uniformly distributed (i.e., if a simpler representation were used), the zonal-mean effect of Kelvin waves on the GW drag would probably be negligible due to cancellation of the effect between phases. In this study, a unique, prognostic GW parameterization (MS-GWaM) is used, which represents the transient GW dynamics in a realistic manner. The role of the transient dynamics in GW drag and QBO evolution in the tropics will have to be investigated in the future.

Acknowledgments
Young-Ha Kim and Ulrich Achatz thank the German Federal Ministry of Education and Research (BMBF) for partial support through the program Role of the Middle Atmosphere in Climate (ROMIC II: QUBICC) and through grant 01LG1905B. Ulrich Achatz thanks the German Research Foundation (DFG) for partial support through the research unit Multiscale Dynamics of Gravity Waves (MS-GWaves) and through grants AC 71/8-2, AC 71/9-2, AC 71/10-2, AC 71/11-2, and AC 71/12-2. This work used resources of the Deutsches Klimarechenzentrum (DKRZ) granted by its Scientific Steering Committee (WLA) under project ID bb1097. The version of the ICON model used here is documented in Borchert et al. (2019). MS-GWaM and its code for the use within ICON have been developed at Goethe-Universität Frankfurt am Main and described in the companion papers Bölöni et al. (2021) and Kim et al. (2021). Open access funding enabled and organized by Projekt DEAL.

References

Achatz, U., Ribstein, B., Senf, F., & Klein, R. (2017). The interaction between synoptic-scale balanced flow and a finite-amplitude mesoscale wave field throughout all atmospheric layers: Weak and moderately strong stratification. *Quarterly Journal of the Royal Meteorological Society*, *143*(702), 342–361. https://doi.org/10.1002/qj.2926

Andrews, D. G., Holton, J. R., & Leovy, C. B. (1987). *Middle atmosphere dynamics*. Academic.

Baldwin, M. P., Gray, L. J., Dunkerton, T. J., Hamilton, K., Haynes, P. H., Randel, W. J., et al. (2001). The quasi-biennial oscillation. *Reviews of Geophysics*, *39*(2), 179–229. https://doi.org/10.1029/1999rg000073

Bergman, J. W., & Salby, M. L. (1994). Equatorial wave activity derived from fluctuations in observed convection. *Journal of the Atmospheric Sciences*, *51*(24), 3791–3806. https://doi.org/10.1175/1520-0469(1994)051<3791:ewadff>2.0.co;2

Bölöni, G., Kim, Y.-H., Borchert, S., & Achatz, U. (2021). Toward transient subgrid-scale gravity wave representation in atmospheric models. Part I: Propagation model including non-dissipative wave-mean-flow interactions. *Journal of the Atmospheric Sciences*, *78*(4), 1317–1338. https://doi.org/10.1175/jas-d-20-0065.1

Booker, J. R., & Bretherton, F. P. (1967). The critical layer for internal gravity waves in a shear flow. *Journal of Fluid Mechanics*, *27*, 513–539. https://doi.org/10.1017/s0022112067000515

Borchert, S., Zhou, G., Baldauf, M., Schmidt, H., Zängl, G., & Reinert, D. (2019). The upper-atmosphere extension of the ICON general circulation model (version: ua-icon-1.0). *Geoscientific Model Development*, *12*(8), 3541–3569. https://doi.org/10.5194/gmd-12-3541-2019

Bushell, A. C., Anstey, J. A., Butchart, N., Kawatani, Y., Osprey, S. M., Richter, J. H., et al. (2020). Evaluation of the quasi-biennial oscillation in global climate models for the SPARC QBO-initiative. *Quarterly Journal of the Royal Meteorological Society*, 3765. https://doi.org/10.1002/qj.3765

Dunkerton, T. J. (1997). The role of gravity waves in the quasi-biennial oscillation. *Journal of Geophysical Research*, *102*(D22), 26053–26076. https://doi.org/10.1029/96jd02999

Holt, L. A., Alexander, M. J., Coy, L., Molod, A., Putman, W., & Pawson, S. (2016). Tropical waves and the quasi-biennial oscillation in a 7-km global climate simulation. *Journal of the Atmospheric Sciences*, *73*(9), 3771–3783. https://doi.org/10.1175/JAS-D-15-0350.1

Holt, L. A., Lott, F., Garcia, R. R., Kiladis, G. N., Cheng, Y. M., Anstey, J. A., et al. (2020). An evaluation of tropical waves and wave forcing of the QBO in the QBOi models. *Quarterly Journal of the Royal Meteorological Society*, 3827. https://doi.org/10.1002/qj.3827

Holton, J. R., & Lindzen, R. S. (1972). An updated theory for the quasi-biennial cycle of the tropical stratosphere. *Journal of the Atmospheric Sciences*, *29*(6), 1076–1080. https://doi.org/10.1175/1520-0469(1972)029<1076:autftq>2.0.co;2

Kim, Y.-H., Bölöni, G., Borchert, S., Chun, H.-Y., & Achatz, U. (2021). Toward transient subgrid-scale gravity wave representation in atmospheric models. Part II: Wave intermittency simulated with convective sources. *Journal of the Atmospheric Sciences*, *78*(4), 1339–1357. https://doi.org/10.1175/jas-d-20-0066.1

Kim, Y.-H., & Chun, H.-Y. (2015). Contributions of equatorial wave modes and parameterized gravity waves to the tropical QBO in HadGEM2. *Journal of Geophysical Research: Atmospheres*, *120*(3), 1065–1090. https://doi.org/10.1002/2014JD022174

Lane, T. P., & Moncrieff, M. W. (2008). Stratospheric gravity waves generated by multiscale tropical convection. *Journal of the Atmospheric Sciences*, *65*(8), 2598–2614. https://doi.org/10.1175/2007jas2601.1

Lindzen, R. S., & Holton, J. R. (1968). A theory of the quasi-biennial oscillation. *Journal of the Atmospheric Sciences*, *25*, 1095–1107. https://doi.org/10.1175/1520-0469(1968)025<1095:atotqb>2.0.co;2

Lott, F., Kuttippurath, J., & Vial, F. (2009). A climatology of the gravest waves in the equatorial lower and middle stratosphere: Method and results for the ERA-40 re-analysis and the LMDz GCM. *Journal of the Atmospheric Sciences*, *66*(5), 1327–1346. https://doi.org/10.1175/2008JAS2880.1

Maury, P., Lott, F., Guez, L., & Duvel, J. P. (2013). Tropical variability and stratospheric equatorial waves in the IPSLCM5 model. *Climate Dynamics*, *40*(9–10), 2331–2344. https://doi.org/10.1007/s00382-011-1273-0

Muraschko, J., Fruman, M. D., Achatz, U., Hickel, S., & Toledo, Y. (2015). On the application of Wentzel-Kramer-Brillouin theory for the simulation of the weakly nonlinear dynamics of gravity waves. *Quarterly Journal of the Royal Meteorological Society*, *141*(688), 676–697. https://doi.org/10.1002/qj.2381

Ortland, D. A., Alexander, M. J., & Grimsdell, A. W. (2011). On the wave spectrum generated by tropical heating. *Journal of the Atmospheric Sciences*, *68*(9), 2042–2060. https://doi.org/10.1175/2011JAS3718.1

Pahlavan, H. A., Fu, Q., Wallace, J. M., & Kiladis, G. N. (2020). Revisiting the quasi biennial oscillation as seen in ERA5. Part I: Description and momentum budget. *Journal of the Atmospheric Sciences*. https://doi.org/10.1175/JAS-D-20-0248.1

Plumb, R. A. (1977). The interaction of two internal waves with the mean flow: Implications for the theory of the quasi-biennial oscillation. *Journal of the Atmospheric Sciences*, *34*(12), 1847–1858. https://doi.org/10.1175/1520-0469(1977)034<1847:tiotiw>2.0.co;2

Ryu, J.-H., Lee, S., & Son, S.-W. (2008). Vertically propagating Kelvin waves and tropical tropopause variability. *Journal of the Atmospheric Sciences*, *65*(6), 1817–1837. https://doi.org/10.1175/2007JAS2466.1

Stockdale, T., Kim, Y.-H., Anstey, J., Palmeiro, F., Butchart, N., Scaife, A., et al. (2020). Prediction of the quasi-biennial oscillation with a multi-model ensemble of QBO-resolving models. *Quarterly Journal of the Royal Meteorological Society*. https://doi.org/10.1002/qj.3919

Wallace, J. M., & Kousky, V. E. (1968). Observational evidence of Kelvin waves in the tropical stratosphere. *Journal of the Atmospheric Sciences*, *25*, 900–907. https://doi.org/10.1175/1520-0469(1968)025<0900:oeokwi>2.0.co;2

Wheeler, M., Kiladis, G. N., & Webster, P. J. (2000). Large-scale dynamical fields associated with convectively coupled equatorial waves. *Journal of the Atmospheric Sciences*, *57*(5), 613–640. https://doi.org/10.1175/1520-0469(2000)057<0613:lsdfaw>2.0.co;2

Yang, G.-Y., Hoskins, B., & Gray, L. (2012). The influence of the QBO on the propagation of equatorial waves into the stratosphere. *Journal of the Atmospheric Sciences*, *69*, 2959–2982. https://doi.org/10.1175/JAS-D-11-0342.1

Zängl, G., Reinert, D., Rípodas, P., & Baldauf, M. (2015). The ICON (ICOsahedral Non-hydrostatic) modelling framework of DWD and MPI-M: Description of the non-hydrostatic dynamical core. *Quarterly Journal of the Royal Meteorological Society*, *141*(687), 563–579. https://doi.org/10.1002/qj.2378